Ultrasound in Medicine & Biology 51 (2025) 312–320

Contents lists available at ScienceDirect

Ultrasound in Medicine & Biology

journal homepage: www.elsevier.com/locate/ultrasmedbio

Original Contribution

Boiling Histotripsy in *Ex Vivo* Human Brain: Proof-of-concept

Ekaterina Ponomarchuk [a,*], Sergey Tsysar [a], Alexey Kadrev [b,c], Anastasia Kvashennikova [a], Daria Chupova [a], Polina Pestova [a], Liliya Papikyan [a], Maria Karzova [a], Natalia Danilova [b], Pavel Malkov [b], Andrey Chernyaev [d], Sergey Buravkov [e], Oleg Sapozhnikov [a], Vera Khokhlova [a]

[a] *Physics Faculty, Lomonosov Moscow State University, Moscow, Russia*
[b] *Medical Research and Educational Center, Lomonosov Moscow State University, Moscow, Russia*
[c] *Diagnostic Ultrasound Division, Russian Medical Academy of Continuous Professional Education, Moscow, Russia*
[d] *Pulmonology Scientific Research Institute, Moscow, Russia*
[e] *Lomonosov Moscow State University, Faculty of Fundamental Medicine, Moscow, Russia*

ARTICLE INFO

Keywords:
HIFU
Boiling histotripsy
Non-invasive surgery
Brain
Neurosurgery

ABSTRACT

Objective: Non-invasive surgical approaches, including boiling histotripsy (BH), are currently being developed for the treatment of brain disorders aiming to avoid craniotomy and exposure of intervening tissues, and, thus, minimize associated complications. This work aimed to demonstrate the feasibility of BH for mechanical fractionation of human brain tissues *ex vivo* under B-mode guidance, with preliminary measurements of tissue stiffness *via* shear wave elastography.

Methods: Young's moduli of 25 human autopsy brain samples obtained from de-identified patients of 51–91 y old (median 77 y old) were measured *via* shear wave elastography prior to BH sonication. Seventeen volumetric BH lesions (1–4 layers of 5 × 5 points with a 1- mm step) were produced near brain surface ($n = 10$), in white matter ($n = 3$), in thalamus ($n = 2$), and globus pallidus ($n = 2$) using 12 element 1.5 MHz sector transducer under B-mode guidance with 10 ms or 2 ms pulses delivered 10 or 15 times per sonication point with 1% duty cycle. After treatment, the lesions were evaluated grossly through bisection, histologically with hematoxylin and eosin staining, and ultrastructurally *via* scanning and transmission electron microscopy.

Results: Young's moduli of autopsy brain samples were lower in older patients (from 32.9 ± 6.6 kPa in 51 y olds to 10 ± 2 kPa in 91 y olds) and at higher temperature (6%–50% lower at 37°C *vs* 23°C), and were within the range observed clinically. All tested BH treatments performed near the brain surface (i.e., mostly in gray matter) resulted in formation of well-demarcated rectangular lesions with homogenized content and sharp boundaries, with majority of residual fragments below 100 microns. The use of shorter pulses (2 ms *vs* 10 ms) accelerated the treatment at least threefold, and the highest liquefaction rate was 568 mm^3/min. White matter was more resistant to BH *vs* gray matter: at least 15 pulses of 2 ms duration were required per each sonication point, and the liquefaction rate was three times lower. The ability of BH to produce lesions in thalamus and globus pallidus was also confirmed.

Conclusion: This work presents the first demonstration of BH proof-of-concept in human brain tissues *ex vivo* under B-mode guidance with clinically relevant treatment rates.

Introduction

Standard protocols for radical management of brain diseases currently include chemotherapy and surgical resection of the target area, which involves craniotomy and incision made through healthy tissues on the way to the target region. Thus, resection of most brain tumors is associated with a high risk of infection, bleeding and other complications, and the surgery outcome highly depends on the tumor size and location in the brain. Minimally invasive procedures, such as endoscopic surgery [1], cryoablation [2] and radiofrequency ablation [3] allow to reduce the craniotomy size and shorten the post-operative recovery period; however, they still require removal of the skull bone and exposure of the intervening tissues to reach the target area. Radiation therapy can allow completely non-invasive ablation of the target tissue transcranially; however, it uses ionizing radiation that affects healthy intervening tissue on the way to the target area and is known to have a cumulative effect on the entire body [4].

Focused ultrasound examination has been suggested as a non-invasive approach to treat brain disorders, for example, to enhance targeted drug delivery through sonoporation and, thus, reduce the required drug

* Corresponding author. Ekaterina Ponomarchuk, Leninskie Gory, 1-2, Moscow, Russian Federation, 119991.
E-mail address: ponomarchuk.em14@physics.msu.ru (E. Ponomarchuk).

https://doi.org/10.1016/j.ultrasmedbio.2024.10.006
Received 3 July 2024; Revised 26 August 2024; Accepted 7 October 2024

doses or use ultrasound-released drugs [5]. Furthermore, high-intensity focused ultrasound (HIFU) modalities provide a non-invasive approach to treat brain disorders by heating the target tissue up to the temperatures of thermal necrosis under magnetic resonance imaging guidance [6]. Thermal HIFU technology is already approved by the U.S. Food and Drug Administration to treat essential tremor and Parkinson's disease by ablating a region in thalamus [7] or globus pallidus [8], both of which are located in the central region of the brain, and is currently undergoing clinical trials for the treatment of other neurological disorders and brain tumors [9]. Such heating-based HIFU modality, however, is known to have certain limitations, including heat sinking and heat diffusion beyond the focal spot that reduce the ablation precision, as well as a reliance on rather costly magnetic resonance imaging guidance. Moreover, the semispherical shape of the current clinical system (ExAblate, Insightec, Inc., Tirat Carmel, Israel) and significant attenuation and distortion of the ultrasound beam on the way through skull bones limit the available area of ablation to the central region of the brain and can result in overheating of the skull and low treatment rate of volumetric targets [10].

A newer HIFU-based modality, termed *histotripsy* [11,12], is currently being developed for neurosurgical purposes as an alternative to thermal HIFU methods. Instead of heating the tissue with continuous ultrasound exposure, histotripsy uses short (microseconds- to milliseconds-long) ultrasound pulses of much higher amplitude containing shock fronts at the focus to fractionate the target tissue mechanically into non-viable suspension. The underlying mechanisms involve gas and vapor bubble activity in the treated area that are highly reflective of ultrasound, which allows the use of conventional B-mode imaging to monitor the treatment.

Intrinsic threshold histotripsy relies on initiation of cavitation within the focal area in tissue by focusing microseconds-long pulses with a greater than 26 MPa peak negative pressure at the focus [11]. The method is being investigated currently for non-invasive neurosurgery on *in vivo* rat and pig models [13–15], as well as for endoscopic procedures [16]. First *in vivo* studies have shown that histotripsy brain treatment results in minor to no bleeding which resolves within 1 wk after treatment. However, this type of histotripsy requires significant negative pressures to be reached at the focus, and therefore, relies on the use of rather large strongly focused transducers. Although the use of multi-element arrays allows expansion of the effective area of treatment *via* electronic steering of the focus [14], the large form factor of intrinsic threshold histotripsy transducers still limits the range of focus positions within the brain.

Boiling histotripsy (BH) uses longer (milliseconds-long) ultrasound pulses to initiate rapid and highly localized tissue boiling within each pulse. BH is feasible with lower acoustic pressures produced at the focus and, therefore, can be realized using more compact transducers than that required for intrinsic threshold histotripsy. This allows the use of less focused arrays for BH that have higher degree of freedom in terms of their positioning relative to the patient's head, thus increasing the available treatment envelope in the brain [17].

Moreover, BH individual lesions are typically larger than those produced *via* cavitation-based histotripsy; therefore, BH treatment rates are typically higher [18,19]. Therefore, although intrinsic threshold histotripsy that produces more compact lesions can be favorable for the treatment of smaller targets, BH may provide a more suitable option for non-invasive resection of large target volumes and accelerate their treatment.

Although it has been shown numerically that the shock amplitudes required for BH brain treatment are achievable when focusing through a human skull [17], the feasibility of BH for human brain ablation has not been investigated experimentally yet. Thus, this study was aimed at the first experimental demonstration of BH feasibility in human brain tissues *ex vivo*. The study consisted of two parts. In the first part, the stiffness (i.e., Young's modulus) of autopsy brain samples was measured *via* a shear wave elastography (SWE) method to confirm their clinical relevance in terms of the stiffness, which is currently considered as the main metric of tissue resistance to BH [18]. In the second part, we aimed to show the ability of BH to generate lesions in tissues located in different parts of the brain: near the brain surface where gray and white matter merge, specifically within the white matter, as well as in thalamus or globus pallidus, which are currently ablated clinically *via* thermal HIFU technique to treat essential tremor and Parkinson's disease [7,8].

Methods

Autopsy brain tissue samples

De-identified brain tissue specimens were obtained *via* rapid autopsy (<24 after death, IRB exempt) from 14 anonymous patients 51–91 y olds (median, 77 y old): 7 males and 7 females. The specimens were then dissected into smaller samples (Fig. 1a–h) and divided into three groups: 13 samples were used, first, for SWE measurements and then sonicated with BH, 12 samples were only used for SWE measurements, and 4 samples were only used for BH. All brain samples were used within 24 h after autopsy.

SWE measurements

Young's moduli of 25 brain tissue samples were measured on Aplio i800 system (Canon, Tokyo, Japan) using linear 14L5 probe in Thyroid preset. The measurements were performed in a plastic container filled with phosphate-buffered saline on a 4 cm high silicone absorbing layer (ToolDecor 25, BMP Technology, Moscow, Russia). At least three measurements were performed in each sample in 4 mm circle areas: 13 samples were measured near brain surface at 1 cm depth (Fig. 1i) at 23°C, 8 samples were used to measure white matter stiffness (Fig. 1j) at 23°C *vs* 37°C, and stiffness of thalamus and globus pallidus were measured in 2 samples each (Fig. 1k, 1l).

The measured values of Young's moduli were compared across different patients with regard to their age and across varied temperatures for each sample individually *via* two-tailed two-sample homoscedastic Student's *t*-test. The significance threshold was set at $p = 0.05$.

BH setup and protocols

Before sonication, 15 brain samples were subjected to 2.5 cycles of alternating degassing (30 min each) and compression (15 min each), and embedded into a 1.5% agarose gel (UltraPure Agarose, Invitrogen, Carlsbad, CA, USA) for the ease of sample positioning during the BH treatment (Fig. 2a). Ten samples were sonicated through gyri near the brain surface at 1 cm depth where typically gray and white matter merged (Fig. 1a, 1e, 1i), 3 samples were used to treat solely white matter without gyri on the beam path (Fig. 1b, 1f, 1j), and 2 lesions were produced per thalamus (Fig. 1c, 1g, 1k) and globus pallidus (Fig. 1d, 1h, 1l). Overall, 17 volumetric BH lesions were produced.

The BH treatments were performed in 34°C water degassed for 3 h with PA WTS (water treatment system, Precision Acoustics, Dorchester, UK) using a 12 element 1.5 MHz sector transducer described in [20], with a 6 cm focal length, an 8 cm outer diameter and a 2 cm central opening diameter (Fig. 2a). The B-mode guidance of the treatment was performed using an L7-4 ultrasound probe (ATL, Philips, Cambridge, MA, USA) positioned on the side of the sample and aligned with the treatment plane (Fig. 2a).

One volumetric lesion per sample was produced by sonication of a 3-D grid of points at an average depth of 1 cm (Fig. 2b). The grid consisted of 1–4 layers, 5 × 5 points each, with a 1 mm increment in all directions as was successfully performed in human prostate and leiomyoma tissues [20,21]. Relative movement of the BH focus and tissue sample was performed by mechanical movement of the agarose-embedded sample attached to a 3-D positioning system (UMS3, Precision Acoustics, UK). Each point of the grid was sonicated with 10-ms or 2-ms pulses with

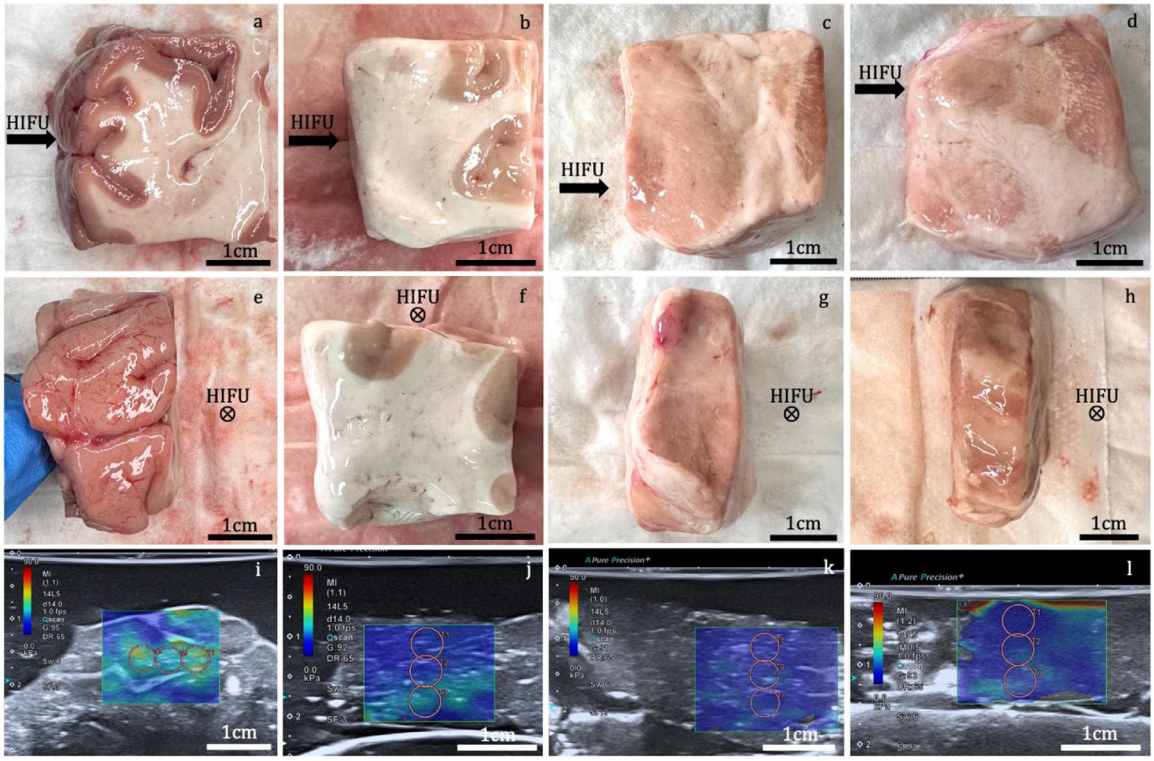

Figure 1. Illustration of sample orientation for boiling histotripsy (BH) and shear wave elastography (SWE) of tissue near brain surface (a, e, i), white matter (b, f, j), thalamus (c, g, k), and globus pallidus (d, h, l). Samples before embedding into agarose gel: high-intensity focused ultrasound (HIFU) incident from the left (a–d), HIFU incident from the observer (e–h) (⊗). Representative SWE images of the brain samples (i–l). Scale bars, 1 cm.

10 or 15 pulses per point (*ppp*). In this pilot study, the treatments were performed at the maximum achievable output voltage driving the transducer (U = 240 V) to ensure successful fractionation of brain tissue. Boiling of the tissue at the selected output voltage was confirmed experimentally by the appearance of a hyperechoic spot on the B-mode during BH treatment, indicating formation of boiling bubbles in the focal area in tissue.

Estimation of shock wave parameters in situ

Experimental peak acoustic pressures and the amplitude of the shock front in brain tissue at the selected voltage were evaluated *via* numerical simulations in the HIFU beam software [22] as described in [20] in a "water–brain" flat-layered medium with the focus positioned 1 cm under the tissue surface. Acoustic properties of brain tissue required for modeling were taken from the literature [23]: density ρ = 1046 kg/m^3, speed of sound c = 1546.3 m/s, nonlinearity coefficient β = 4.36, diffusivity coefficient δ = 4.33 mm^2/s, absorption coefficient α = 0.106 Np/cm at a 1.5 MHz frequency, with power law ν = 1.1. The calculated peak positive pressure field around the focus and the focal pressure waveform are shown in Figure 3. The axial and lateral dimensions of the focal spot at the selected voltage (i.e., in non-linear regime) were 4.7 mm × 0.42 mm at −3 dB peak positive pressure, and 12.2 mm × 1.7 mm at zero pressure (Fig. 3a). The maximum achievable shock wave parameters at the focus were as follows: peak positive and negative pressures were 138 and −24 MPa, respectively, and the shock amplitude was 155 MPa (Fig. 3b). The time to reach tissue boiling, given the heat capacity per unit volume of brain tissue c_v = 3.8 MJ/(m^3·K) [23], was evaluated according to the standard procedure based on the energy absorption at the shock fronts [12,24]: $t_b = \Delta T c_v 6\rho^2 c^4/(\beta f_0 A_s^3)$, where ΔT is the temperature change from the tissue temperature to the boiling temperature, f_0 is the ultrasound frequency, and A_s is the shock amplitude at the focus.

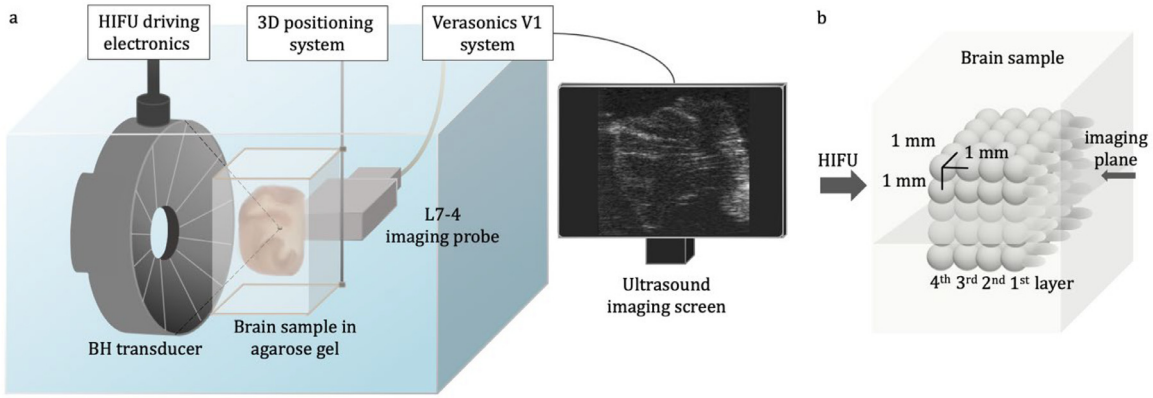

Figure 2. (a) Experimental setup for boiling histotripsy (BH) ablation of agarose-embedded brain tissue samples *ex vivo*. (b) Schematics of the sonication geometry for generation of a volumetric lesion in a brain tissue sample. HIFU, high-intensity focused ultrasound.

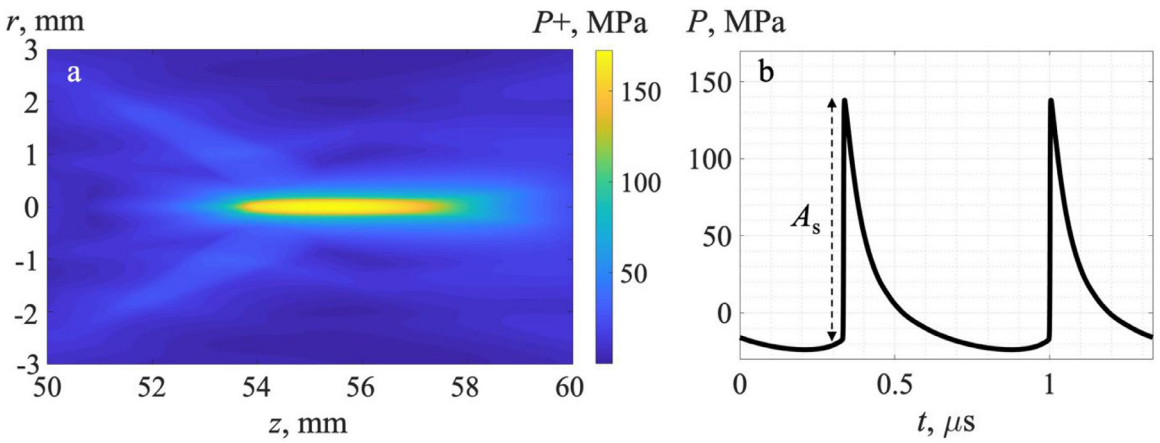

Figure 3. Numerically calculated shock wave field *in situ*. (a) Distribution of peak positive pressure amplitude in the axial plane around the focus, (b) two cycles of the pressure waveform at the focus. A_s, shock amplitude.

Thus, the time to reach tissue boiling was shown to be 0.44 ms, that is, within each BH pulse, as required for BH. However, the simulations did not account for any inhomogeneities on the beam path, and numerically predicted shock wave parameters could be overestimated and boiling time—underestimated. Therefore, the tissue boiling within the intended BH pulse was confirmed experimentally on the B-mode as described elsewhere in this article.

Microscopic analysis of BH outcome

After treatment, the obtained volumetric lesions were investigated *via* B-mode imaging, then 11 lesions were bisected along the imaging plane for gross analysis, and the other 6 lesions were marked with histological inks (HistoSafe, Moscow, Russia), fixed *en bloc* in 10% neutral buffered formalin (Labiko, St. Petersburg, Russia), cut into 2 mm thick sections parallel to the imaging plane, processed and embedded in paraffin. Then, 3 μm thick sections were taken from the resulting blocks, processed and stained with hematoxylin and eosin for histological evaluation of the BH outcome by a certified pathologist (N.D.).

Lesion volumes were estimated as a product of three dimensions measured either grossly after bisection, or in histological slides. The liquefaction rate was then evaluated as the lesion volume divided by the treatment time.

The content of 7 of 11 bisected lesions was collected with a scalpel and either placed on a carbon double-sided tape and prepared for scanning electron microscopy (SEM) as described in [24], or diluted with distilled water to separate individual residual fragments, and processed for SEM or transmission electron microscopy (TEM) as described in [25]. SEM specimens containing diluted lesion content were digitalized on JEOL JSM-6380LA Analytical Scanning Electron Microscope (Tokyo, Japan), and maximum Feret diameters of all residual fragments of brain tissue exceeding 20 μm were measured in ImageJ software (National Institutes of Health, Bethesda, MD, USA). A two-tailed two-sample Student's *t*-test was performed to compare the measured values of fragment sizes across varied BH protocols and brain tissues. Overall, 2786 residual fragments were analyzed. Significance threshold was set at $p = 0.05$. TEM specimens were digitalized on JEOL JEM-1011 Transmission Electron Microscope (Tokyo, Japan).

Results

Stiffness of autopsy brain tissue samples

Figure 4a shows Young's moduli measured *via* SWE near the brain surface through gyri at 1 cm depth for patients of different age and sex. The autopsy samples of younger patients were statistically stiffer, as per Student's *t*-test, which agrees with the literature [26–28]. SWE measurements of white matter in samples kept at 23°C *vs* heated up to 37°C (Fig. 4b) showed that brain stiffness decreased with temperature, as per Student's *t*-test, which also agrees with the literature [29]. Specifically,

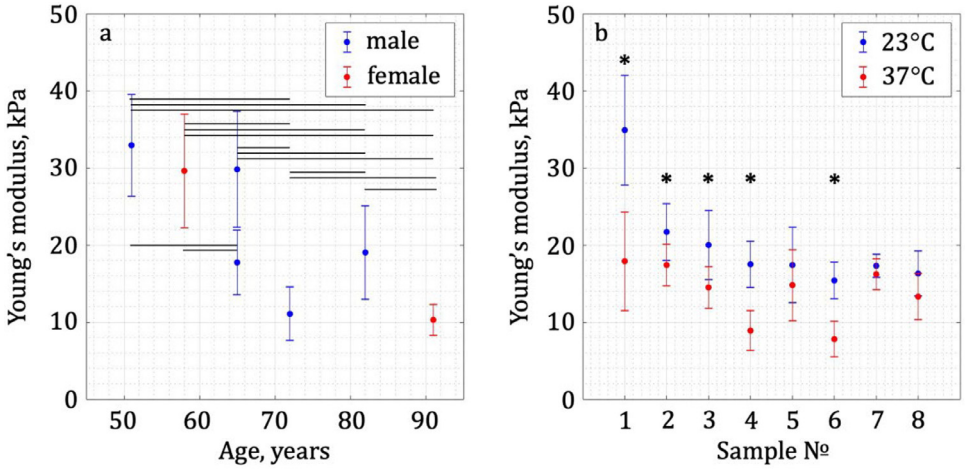

Figure 4. Young's moduli in *ex vivo* human brain tissue samples. (a) Measured 1 cm under brain surface (see Fig. 1i) at 23°C in dependence on the patient age, (b) measured in white matter (see Fig. 1j) at 23°C *vs* 37°C. Data represents mean values; error bars represent standard deviations, horizontal lines in (a) and asterisk marks in (b) indicate statistically significant difference, as per Student's *t*-test.

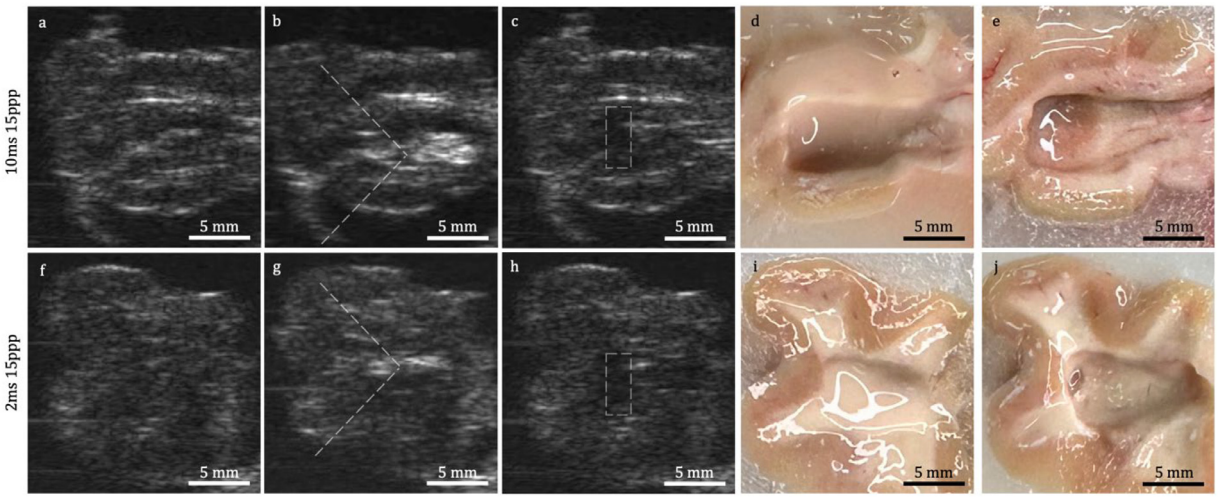

Figure 5. B-mode images and gross photographs after bisection of the brain samples treated with (10 ms 15 ppp) (*top row*) and (2 ms 15 ppp) (*bottom row*). B-mode images before (a, f), during (b, g), and after (c, h) the treatment. Dashed lines in (b, g) indicate the geometry of the boiling histotripsy (BH) beam. Dashed boxes in (c, h) outline the target area (i.e., targeted grid + 1 mm laterally and axially). Gross photographs after lesion bisection before (d, i) and after (e, j) rinsing the lesion with phosphate-buffered saline. Scale bars, 5 mm. High-intensity focused ultrasound (HIFU) incident from the left.

Young's modulus range in autopsy white matter was 15.4–34.9 kPa at 23°C and 8.9–17.9 kPa at 37°C, being within the broad range reported in literature [26,30]. The Young's modulus of thalamus and globus pallidus at 23°C were statistically similar: 13.8 ± 3.2 kPa and 12.4 ± 3.6 kPa, respectively. All stiffness values obtained here were within the typical range observed clinically [26,30], which confirms clinical relevance of the autopsy brain samples used here in *ex vivo* studies.

BH outcome near brain surface

Representative B-mode images of the brain samples before, during and after the BH treatment are shown in Figure 5 (a–c, f–h) and Figure 6 (a–c, f–h). The ultrasound guidance of the BH treatment process in all samples was successful: the area being treated appeared hyperechoic on the B-mode during the treatment. After treatment, the treated area appeared hypoechoic indicating liquefaction of the target volume.

Localization of the treated volume observed after bisection correlated well with that visible on the B-mode (Fig. 5d, 5e, 5i, 5j). The obtained BH lesions after bisection had rectangular shape, and the lesion dimensions exceeded the target grid by 1.0–1.3 mm laterally, and by up to 7 mm axially, which is typical for BH [24]. Both BH protocols using 10 ms and 2 ms pulses with 15 ppp resulted in formation of well-demarcated lesions with liquid content (Fig. 5d, 5i) easily removed by rinsing the lesion with phosphate-buffered saline (Fig. 5e, 5j). Estimation of the liquefaction rate showed that the use of shorter pulses, 2 ms *vs* 10 ms, with the same number of pulses per point (15 ppp) allowed for at least threefold treatment acceleration from 68 ± 56 mm^3/min to 183 ± 67 mm^3/min. The maximum liquefaction rate achieved within the tested parameter range was obtained using 2 ms pulses with 10 ppp and was 568 mm^3/min.

Figure 6 (c, d, g, h) shows hematoxylin and eosin-stained histological sections of the lesions produced in brain samples using short pulses (2 ms) with varied number of pulses per point (15 and 10 ppp). Histologically, both lesions appeared as homogenous suspension showing loss of cellular structure with residual non-viable basophilic nuclei debris. The lesions in both regimes were sharply demarcated with a clear boundary between treated and intact tissue and were surrounded by viable brain tissue cells immediately adjacent to completely fractionated cells (Fig. 6e, 6j). Lesion dimensions and corresponding liquefaction rates estimated from histological sections were lower than those evaluated

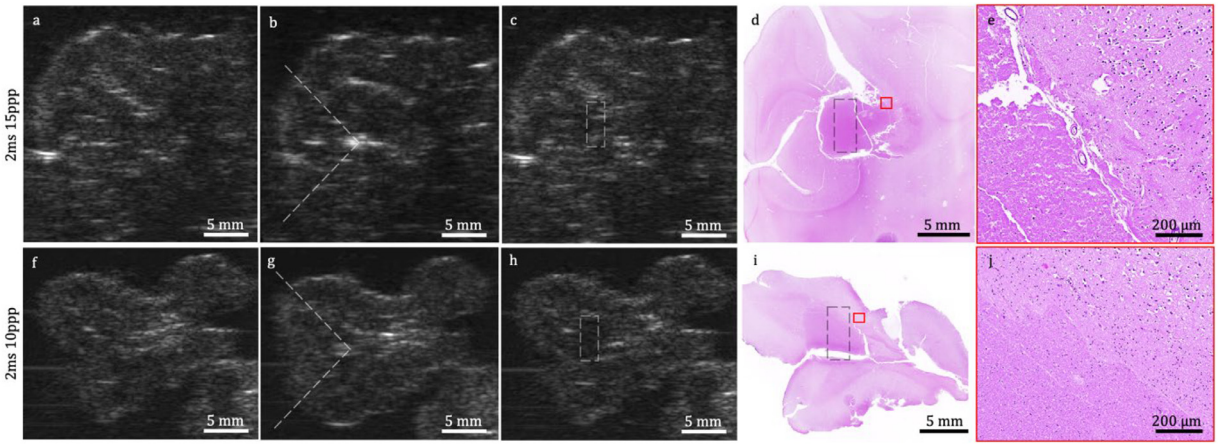

Figure 6. B-mode images and histological sections of the brain samples treated with (2 ms 15 ppp) (*top row*) and (2 ms 10 ppp) (*bottom row*). B-mode images before (a, f), during (b, g), and after (c, h) the treatment. Histotopograms of the brain samples containing volumetric boiling histotripsy (BH) lesions (d, i), lesion border (*red boxes*) under higher magnification (e, j). High-intensity focused ultrasound incident from the left. Dashed lines in (b, g) indicate the geometry of the BH beam. Dashed boxes in (c–d, h–i) outline the target area (i.e., target grid + 1 mm laterally and axially).

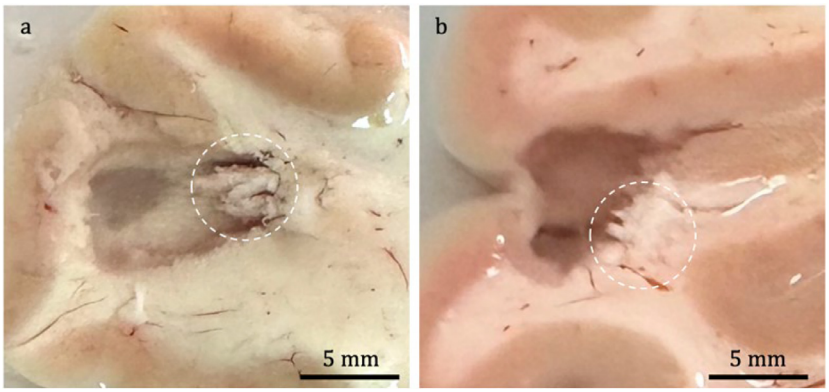

Figure 7. Gross photographs after lesion bisection illustrating higher resistance of white matter to boiling histotripsy *vs* gray matter: *dashed circles* outline incomplete damage of white matter in distal part of the lesion. High-intensity focused ultrasound incident from the left. Scale bars, 5 mm.

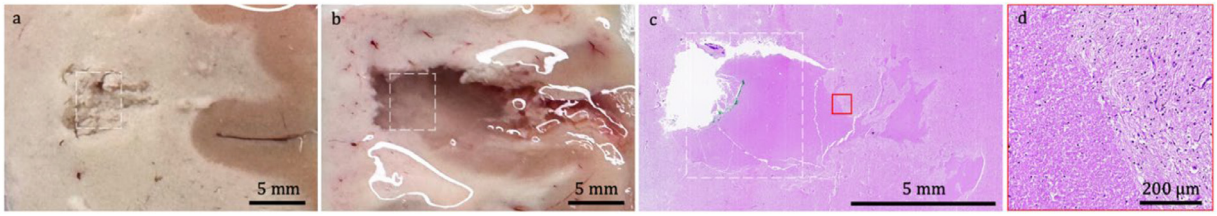

Figure 8. Volumetric boiling histotripsy lesions produced in white matter using (a) 2 ms 10 ppp, (b–d) 2 ms 15 ppp. (a, b) Gross photographs after lesion bisection along the imaging plane, (c) histotopogram, and (d) lesion border (*red box*) under higher magnification. High-intensity focused ultrasound incident from the left. Dashed boxes outline the target area (i.e., target grid + 1 mm laterally and axially).

grossly from bisected lesions due to a well-known shrinkage effect during formalin fixation [29]. The liquefaction rates for (2 ms 15 ppp) and (2 ms 10 ppp) regimes estimated from histology were similar 105 and 92 mm^3/min, respectively.

BH outcome in white matter

In some cases, when white matter was located in the distal part of the sonicated volume, incomplete fractionation of white matter was observed (dashed circles in Fig. 7), possibly implying higher resistance of white matter to BH *vs* gray matter. This was also confirmed by a series of white matter treatments (Fig. 8). The BH protocol (2 ms 10 ppp), which was shown to be sufficient to successfully fractionate mostly gray matter near the brain surface (Fig. 6f–j), resulted in incomplete damage of white matter (Fig. 8a). A higher number of pulses per point (15 ppp) was required to produce homogenous volumetric lesion in white matter (Fig. 8b–d), and lower liquefaction rate was achieved in white *vs* gray matter given the same pulsing protocol (2 ms 15 ppp): 59 mm^3/min *vs* 183 mm^3/min.

BH outcome in thalamus and globus pallidus

Volumetric BH lesions in thalamus and globus pallidus were produced using 2 ms pulses with 15 ppp (Fig. 9), and histologically revealed homogenization of the brain matter in the treated area (Fig. 9iv) as opposed to intact tissue outside the lesion (Fig. 9v). In agreement with

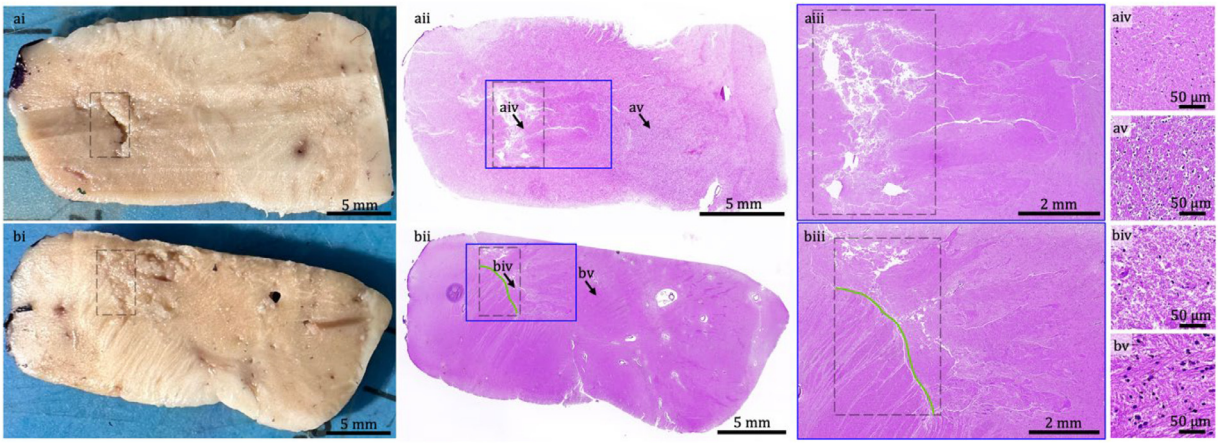

Figure 9. Volumetric boiling histotripsy lesions produced in (a) the thalamus and (b) globus pallidus: (i) macroscopic image of the treated sample after formalin fixation and bisection along the imaging plane, (ii) histotopograms, (iii) magnified area containing the lesion, (iv) magnified area within the lesion, and (v) magnified intact area. high-intensity focused ultrasound (HIFU) incident from the left. *Dashed boxes* outline the target area (i.e., target grid + 1 mm laterally and axially). Green curves in (bii) and (biii) outline the border between the intact white matter and the lesion.

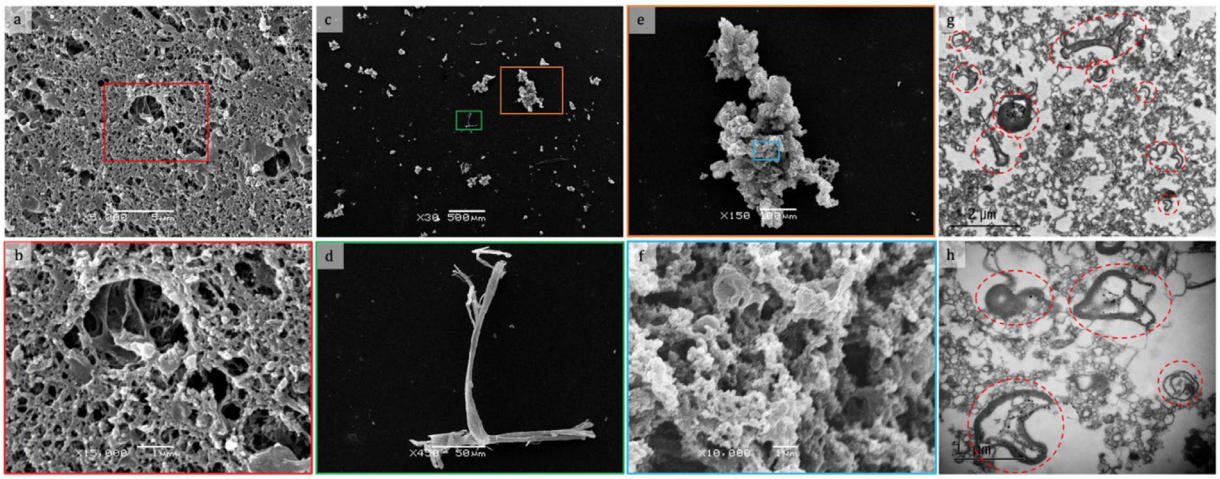

Figure 10. Representative electron microscopy images: scanning electron microscopy of undiluted (a, b) and diluted (c–f) lesion content, transmission electron microscopy of diluted lesion content (g, h). *Dashed circles* in (g, h) outline damaged myelin fragments.

higher resistance of white matter to BH observed above, the lesion in globus pallidus was confined within its gray matter (green curve in Fig. 9bii, biii) and spared the white matter immediately adjacent to globus pallidus. Liquefaction rates in thalamus and globus pallidus estimated from histology were lower than that obtained in gray or white matter: 7 and 28 mm^3/min in thalamus and globus pallidus, respectively, but their optimization was beyond the scope of this study.

Ultrastructural analysis of the lesion content

Figure 10 shows representative images of BH lesion content obtained *via* SEM and TEM. Undiluted lesion content revealed multi-layered fragments of mechanically damaged brain matter and structureless cellular components (Fig. 10a, 10b). Dilution of the lesion content in distilled water allowed distribution of residual tissue fragments over the substrate, and thus analyze them individually and measure their dimensions (Fig. 10c). Individual residual debris appeared either as damaged nerve fibers (Fig. 10d) or as aggregates of structureless cellular components (Fig. 10e, 10f). TEM confirmed BH-induced loss of cellular structure and revealed components of fractionated cells (damaged nuclei and organelles) and damaged myelin fibers (Fig. 10g, 10h).

Quantitative analysis of brain tissue fragments remaining after BH treatment showed that, regardless of BH protocol, the majority of residual debris (>90% across all lesions) did not exceed 100 microns in length, and the average and median sizes across all lesions were 46 and 26 microns, respectively. The largest fragment remaining after BH was a piece of damaged nerve fiber 1187 microns long. No statistically significant difference in residual fragment sizes in gray *vs* white matter was observed. With regard to the BH protocol, on average, smaller fragments remained after the use of lower ppp with a fixed pulse duration, that is, (2 ms 10 ppp) *vs* (2 ms 15 ppp) and (10 ms 10 ppp) *vs* (10 ms 15 ppp).

Discussion

The results of this work represent the first demonstration of BH feasibility for non-invasive mechanical fractionation of human brain tissue *ex vivo* under ultrasound guidance. In autopsy human brain samples, with SWE-measured Young's moduli within the clinically observed range, volumetric BH lesions were successfully produced with 10 ms and 2 ms pulses with 10 or 15 pulses per each sonicated point (ppp) of the volumetric grid. The treatments were planned and monitored using conventional B-mode ultrasound imaging, and the liquefaction of the treated volumes was confirmed first on the B-mode, then grossly after lesion bisection, histologically with hematoxylin and eosin staining and ultrastructurally on SEM and TEM.

Young's moduli of autopsy brain tissue samples were found to be within the range reported by others [26,30]. Softening of brain tissue with temperature observed in this study confirmed previously reported results in [31] and implies that susceptibility of brain tissue to BH at physiological temperature in clinical settings may be even higher *vs* that observed in our study, which was performed at 34°C. In comparison with other target tissues for BH ablation, human brain tissue was found to be softer than human prostate tissue previously treated with BH in our recent study [25], and, accordingly, required a lower number of ppp, in agreement with a common pattern of softer tissues having higher susceptibility to BH [18]. Similarly, the Young's moduli of human brain samples were higher *vs* those reported for porcine liver [32], and, respectively, the exposure parameters required here to produce homogenous volumetric lesions in human brain tissue were higher *vs* those reported in our recent study for porcine liver tissue [33].

Here it was shown that shorter BH pulses (2 ms *vs* 10 ms) can be used to accelerate the treatment at least threefold while maintaining a high degree of tissue fractionation as confirmed histologically: treatment time was five times shorter but shorter BH pulses typically produce shorter lesions resulting in smaller lesion volumes. All volumetric treatment rates achieved in this work were equal or higher than those that can be estimated from the intrinsic threshold histotripsy studies [13,14,16], or than currently achieved in clinics *via* thermal transcranial HIFU [34–37]. Higher liquefaction rates obtained in this work in BH regime may be favorable for the treatment of large brain tumors or hematomas that are hard to resect surgically or inoperable due to their size and/or localization. However, the presence of the skull on the ultrasound beam path in transcranial BH application may decrease the BH treatment rate and should be tested and optimized in further studies.

SEM of diluted and centrifuged brain lesion content demonstrated that BH can mechanically fractionate brain tissue into fragments primarily below 100 microns. Higher ppp with a fixed pulse duration left larger damaged tissue fragments post-treatment arguably due to the longer postfocal lesion "tails," which are narrower than the main "heads" of the BH lesions. Such narrow "tails" typically do not merge together and, thus, could have formed larger residual fragments.

White matter was found to be more resistant to BH *vs* gray matter: a higher ppp was required to produce a volumetric lesion with a fixed pulse duration, and treatment rates were lower in white matter given a fixed BH protocol. Although stiffness comparison of white *vs* gray matter within the same sample was beyond the scope of this study, our SWE data for patients of similar age suggest that stiffness near the brain

surface (i.e., of mostly gray matter) was somewhat softer *vs* that of pure white matter, which agrees with the literature [28,38] and may explain the observed higher resistance of white matter to BH. Another possible reason is the high content of nerve fibers in white matter and their anisotropic orientation, because fibrous tissues were shown to have higher resistance to BH [33].

Currently, the most clinically relevant target brain areas considered in this study were thalamus and globus pallidus because their ablation *via* thermal HIFU modalities has been approved by the U.S. Food and Drug Administration and is performed currently to treat essential tremor and Parkinson's disease [7,8]. Here we have shown the ability of BH to generate lesions in the thalamus and globus pallidus under reliable B-mode guidance, which demonstrates the potential of BH to serve as an alternative to thermal HIFU treatment of essential tremor and Parkinson's disease and to eliminate the need to rely on magnetic resonance thermometry, pending further testing and optimization of the BH protocols and ultrasound-based imaging transcranially.

In clinical settings, a lower frequency BH transducer would be more suitable to reduce ultrasound attenuation and achieve sufficient shock amplitudes *in situ* given significant energy attenuation in skull bone [17]. The use of lower ultrasound frequency would result in even larger BH lesions [18] and, therefore, higher ablation rates than those obtained in this study.

Another difference in the clinical implementation of transcranial BH compared with our *ex vivo* study is the significant distortion of the BH beam on the way through the skull bones. However, multi-element arrays for transcranial BH [17,34] are currently being developed to allow for compensation of the possible aberrations based on pre-operative computed tomography or magnetic resonance imaging scans to ensure sharp focusing and formation of shocks with sufficient amplitudes at the focus. It has already been shown in numerical experiments that shock amplitudes sufficient for BH treatment in brain are achievable when focusing through a human skull with the implementation of aberration correction techniques [17]. Moreover, compared with the large, highly focused transducers required for intrinsic threshold histotripsy, such BH arrays are being developed to be more compact and less focused, and, therefore, can be shifted and rotated relative to the patient's skull [17]. This will potentially expand the currently available region for non-invasive ablation in human brain [39], thus allowing for treating not only essential tremor and Parkinson's disease, but also brain tumors, hematomas and stereotactic target points that are often located outside of central part of the brain.

Distortion and attenuation of ultrasound by the skull bones would also pose a challenge for ultrasound transcranial imaging in clinical settings as opposed to our *ex vivo* setup. However, currently developed transcranial ultrasound imaging techniques [40], such as super-resolution imaging [41] and 3-D Ultrasound Matrix Imaging [42], could allow for the ultrasound imaging-based guidance of the BH treatment in further *in vivo* implementation. Moreover, to provide quantitative real-time feedback during BH treatment, a new method is being developed currently based on ultrafast color Doppler measurements to quantify the velocity of the liquefied tissue within the lesion as a candidate metric of treatment completeness [43].

Our study represents the first step toward BH applications in human brain, which included: (1) pilot demonstration of principal ability of BH to fractionate various human brain tissues under the simplest and well-controlled conditions with the absence of the skull, (2) analysis of the corresponding outcomes at macro-, micro- and ultrastructural levels and (3) preliminary protocol optimization in terms of the pulse duration and number of pulses per point. Although it has been shown numerically that the shock waves required to initiate BH can be generated in human brain transcranially with the use of aberration correction algorithms [17], further experiments with the presence of the skull using multi-element arrays are essential to address the challenges of beam aberration and attenuation and to demonstrate the potential of BH for transcranial brain treatment, which was beyond the scope of this study.

In this pilot study, the highest achievable output voltage and a small step size between the volumetric grid points were used to ensure complete fractionation of human brain tissue, based on our previous successful studies in human prostate tissue [20,25]. However, the high quality and large dimensions of the produced BH lesions in brain tissue imply that lower voltage and larger step size might be sufficient for complete liquefaction of brain tissue. Moreover, as the same number of pulses per sonication point was sufficient to achieve the same degree of tissue fractionation using 10 and 2 ms pulses, further optimization of the protocols by decreasing ppp and/or pulse duration can be performed to further accelerate the treatment while maintaining its quality.

Conclusion

This work is the first to support the feasibility of ultrasound-guided BH for non-invasive mechanical fractionation of different human brain tissues *ex vivo* with clinically relevant treatment rates. Overall, based on the promising results obtained here, further optimization of the BH protocols and data collection are ongoing.

Conflict of interest

The authors declare no competing interests.

Data availability

Data will be made available on request.

Acknowledgments

This work was supported by the Russian Science Foundation [grant 20-12-00145] and Moscow State University Program of Development [grant №24-SCH06-12]. Postgraduate students Ekaterina Ponomarchuk and Daria Chupova were supported by student fellowships from Foundation for the Advancement of Theoretical Physics and Mathematics "BASIS" [20-2-10-10-1] and [22-2-10-6-1]. The authors also thank T.I. Milenkovich for assistance in sample preparation for BH treatment and S.A. Usmanova for preparing histological specimens.

References

[1] Rox MF, Ropella DS, Hendrick RJ, Blum E, Naftel RP, Bow HC, et al. Mechatronic design of a two-arm concentric tube robot system for rigid neuroendoscopy. IEEE ASME Trans Mechatron 2020;25:1432–43. doi: 10.1109/tmech.2020.2976897.

[2] Li C, Wu L, Song J, Liu M, Lv Y, Sequeiros RB. MR imaging-guided cryoablation of metastatic brain tumours: initial experience in six patients. Eur Radiol 2010;20:404–9. doi: 10.1007/s00330-009-1554-8.

[3] Gananadha S, Wulf S, Morris DL. Safety and efficacy of radiofrequency ablation of brain: a potentially minimally invasive treatment for brain tumours. Minim Invasive Neurosurg 2004;47:325–8. doi: 10.1055/s-2004-830124.

[4] Coderre JA, Morris GM, Micca PL, Hopewell JW, Verhagen I, Kleiboer BJ, et al. Late effects of radiation on the central nervous system: role of vascular endothelial damage and glial stem cell survival. Radiat Res 2006;166:495–503. doi: 10.1667/RR3597.1.

[5] O'Reilly MA, Hynynen K. Ultrasound enhanced drug delivery to the brain and central nervous system. Int J Hyperthermia 2012;28:386–96. doi: 10.3109/02656736.2012.666709.

[6] Qiu W, Bouakaz A, Konofagou EE, Zheng H. Ultrasound for the brain: a review of physical and engineering principles, and clinical applications. IEEE Trans Ultrason Ferroelectr Freq Control 2021;68:620. doi: 10.1109/TUFFC.2020.3019932.

[7] Cosgrove GR, Lipsman N, Lozano AM, Chang JW, Halpern C, Ghanouni P, et al. Magnetic resonance imaging-guided focused ultrasound thalamotomy for essential tremor: 5-year follow-up results. J Neurosurg 2022;138:1028–33. doi: 10.3171/2022.6.JNS212483.

[8] Krishna V, Fishman PS, Eisenberg HM, Kaplitt M, Baltuch G, Chang JW, et al. Trial of globus pallidus focused ultrasound ablation in Parkinson's disease. N Engl J Med 2023;388:683–93. doi: 10.1056/NEJMoa2202721.

[9] Baek H, Lockwood D, Mason EJ, Obusez E, Poturalski M, Rammo R, et al. Clinical intervention using focused ultrasound (FUS) stimulation of the brain in diverse neurological disorders. Front Neurol 2022;9:880814. doi: 10.3389/fneur.2022.880814.

[10] Pulkkinen A, Huang Y, Song J, Hynynen K. Simulations and measurements of transcranial low-frequency ultrasound therapy: skull-base heating and effective area of treatment. Phys Med Biol 2011;56:4661–83. doi: 10.1088/0031-9155/56/15/003.

[11] Xu Z, Ludomirsky A, Eun LY, Hall TL, Tran BC, Fowlkes JB, et al. Controlled ultrasound tissue erosion. IEEE Trans Ultrason Ferroelectr Freq Control 2004;51:726–36. doi: 10.1109/tuffc.2004.1308731.
[12] Canney MS, Khokhlova VA, Bessonova OV, Bailey MR, Crum LA. Shock-induced heating and millisecond boiling in gels and tissue due to high intensity focused ultrasound. Ultrasound Med Biol 2010;36:250–67. doi: 10.1016/j.ultrasmedbio.2009.09.010.
[13] Sukovich JR, Cain CA, Pandey AS, Chaudhary N, Camelo-Piragua S, Allen SP, et al. *In vivo* histotripsy brain treatment. J Neurosurg 2018;1:1–8. doi: 10.3171/2018.4.JNS172652.
[14] Lu N, Gupta D, Daou BJ, Fox A, Choi D, Sukovich JR, et al. Transcranial magnetic resonance-guided histotripsy for brain surgery: pre-clinical investigation. Ultrasound Med Biol 2022;48:98–110. doi: 10.1016/j.ultrasmedbio.2021.09.008.
[15] Choi SW, Duclos S, Camelo-Piragua S, Chaudhary N, Sukovich J, Hall T, et al. Histotripsy treatment of murine brain and glioma: temporal profile of magnetic resonance imaging and histological characteristics post-treatment. Ultrasound Med Biol 2023;49:1882–91. doi: 10.1016/j.ultrasmedbio.2023.05.002.
[16] Landry TG, Gannon J, Vlaisavljevich E, Mallay MG, Woodacre JK, Croul S, et al. Endoscopic coregistered ultrasound imaging and precision histotripsy: initial *in vivo* evaluation. BME Front 2022;2022:9794321. doi: 10.34133/2022/9794321.
[17] Rosnitskiy PB, Yuldashev PV, Sapozhnikov OA, Gavrilov LR, Khokhlova VA. Simulation of nonlinear trans-skull focusing and formation of shocks in brain using a fully populated ultrasound array with aberration correction. J Acoust Soc Am 2019;146:1786. doi: 10.1121/1.5126685.
[18] Khokhlova TD, Kucewicz JC, Ponomarchuk EM, Hunter C, Bruce M, Khokhlova VA, et al. Effect of stiffness of large extravascular hematomas on their susceptibility to boiling histotripsy liquefaction in vitro. Ultrasound Med Biol 2020;46:2007–16. doi: 10.1016/j.ultrasmedbio.2020.04.023.
[19] Khokhlova TD, Monsky WL, Haider YA, Maxwell AD, Wang YN, Matula TJ. Histotripsy liquefaction of large hematomas. Ultrasound Med Biol 2016;42:1491–8. doi: 10.1016/j.ultrasmedbio.2016.01.020.
[20] Rosnitskiy PB, Tsysar SA, Karzova MM, Buravkov SV, Malkov PG, Danilova NV, et al. Pilot *ex vivo* study on non-thermal ablation of human prostate adenocarcinoma tissue using boiling histotripsy. Ultrasonics 2023;133:107029. doi: 10.1016/j.ultras.2023.107029.
[21] Ponomarchuk E, Tsysar S, Kvashennikova A, Chupova D, Pestova P, Danilova N, et al. Pilot study on boiling histotripsy treatment of human leiomyoma *ex vivo*. Ultrasound Med Biol 2024;50:1255–61. doi: 10.1016/j.ultrasmedbio.2024.05.002.
[22] Yuldashev PV, Karzova MM, Kreider W, Rosnitskiy PB, Sapozhnikov OA, Khokhlova VA. "HIFU Beam:" a simulator for predicting axially symmetric nonlinear acoustic fields generated by focused transducers in a layered medium. IEEE Trans Ultrason Ferroelectr Freq Control 2021;68:2837–52. doi: 10.1109/TUFFC.2021.3074611.
[23] Hasgall PA, Di Gennaro F, Baumgartner C, Neufeld E, Lloyd B, Gosselin MC, et al. IT'IS database for thermal and electromagnetic parameters of biological tissues. Version 4.1. 2022.
[24] Ponomarchuk EM, Rosnitskiy PB, Khokhlova TD, Buravkov SV, Tsysar SA, Karzova MM, et al. Ultrastructural analysis of volumetric histotripsy bio-effects in large human hematomas. Ultrasound Med Biol 2021;47:2608–21. doi: 10.1016/j.ultrasmedbio.2021.05.002.
[25] Khokhlova VA, Rosnitskiy PB, Tsysar SA, Buravkov SV, Ponomarchuk EM, Sapozhnikov OA, et al. Initial assessment of boiling histotripsy for mechanical ablation of *ex vivo* human prostate tissue. Ultrasound Med Biol 2023;49:62–71. doi: 10.1016/j.ultrasmedbio.2022.07.014.
[26] Takamura T, Motosugi U, Sasaki Y, Kakegawa T, Sato K, Glaser KJ, et al. Influence of age on global and regional brain stiffness in young and middle-aged adults. J Magn Reson Imaging 2020;51:727–33. doi: 10.1002/jmri.26881.
[27] Tzschätzsch H, Kreft B, Schrank F, Bergs J, Braun J, Sack I. In vivo time-harmonic ultrasound elastography of the human brain detects acute cerebral stiffness changes induced by intracranial pressure variations. Sci Rep 2018;8:17888. doi: 10.1038/s41598-018-36191-9.
[28] Murphy MC, Huston 3rd J, Ehman RL. MR elastography of the brain and its application in neurological diseases. Neuroimage 2019;187:176–83. doi: 10.1016/j.neuroimage.2017.10.008.
[29] Tran T, Sundaram CP, Bahler CD, Eble JN, Grignon DJ, Monn MF, et al. Correcting the shrinkage effects of formalin fixation and tissue processing for renal tumors: toward standardization of pathological reporting of tumor size. J Cancer 2015;6:759–66. doi: 10.7150/jca.12094.
[30] Morin F, Chabanas M, Courtecuisse H, Payan Y. Biomechanical modeling of brain soft tissues for medical applications. In: Payan Y, Jacques O, editors. Biomechanics of living organs. New York: Academic Press; 2017. p. 127–46. doi: 10.1016/B978-0-12-804009-6.00006-7.
[31] Liu YL, Li GY, He P, Mao ZQ, Cao Y. Temperature-dependent elastic properties of brain tissues measured with the shear wave elastography method. J Mech Behav Biomed Mater 2017;65:652–6 Epub 2016 Sep 21. PMID: 27741495. doi: 10.1016/j.jmbbm.2016.09.026.
[32] Yang C, Yin M, Glaser KJ, Zhu X, Xu K, Ehman RL, et al. Static and dynamic liver stiffness: An ex vivo porcine liver study using MR elastography. Magn Reson Imaging 2017;44:92–5. doi: 10.1016/j.mri.2017.08.009.
[33] Ponomarchuk E, Thomas G, Song M, Krokhmal A, Kvashennikova A, Wang YN, et al. Histology-based quantification of boiling histotripsy outcomes via ResNet-18 network: towards mechanical dose metrics. Ultrasonics 2024;138:107225. doi: 10.1016/j.ultras.2023.107225.
[34] Torii J, Maesawa S, Nakatsubo D, Tsugawa T, Kato S, Ishizaki T, et al. Cutoff values for the best management strategy for magnetic resonance-guided focused ultrasound ablation for essential tremor. J Neurosurg 2022:1–12. doi: 10.3171/2022.3.JNS212460.
[35] Meng Y, Huang Y, Solomon B, Hynynen K, Scantlebury N, Schwartz ML, et al. MRI-guided focused ultrasound thalamotomy for patients with medically-refractory essential tremor. J Vis Exp 2017(130):56365. doi: 10.3791/56365.
[36] Martin E, Werner B, Bauer R, van Leyen K, Coluccia D, Fandino J. Clinical neurological HIFU applications: the Zurich experience. Transl Cancer Res 2014;3:449–58. doi: 10.3978/j.issn.2218-676X.2014.09.01.
[37] Ram Z, Cohen ZR, Harnof S, Tal S, Faibel M, Nass D, et al. Magnetic resonance imaging-guided, high-intensity focused ultrasound for brain tumor therapy. Neurosurgery 2006;59:949–55 discussion 955–6. doi: 10.1227/01.NEU.0000254439.02736.D8.
[38] Budday S, Nay R, de Rooij R, Steinmann P, Wyrobek T, Ovaert TC, et al. Mechanical properties of gray and white matter brain tissue by indentation. J Mech Behav Biomed Mater 2015;46:318–30. doi: 10.1016/j.jmbbm.2015.02.024.
[39] Chupova DD, Rosnitskiy PB, Gavrilov LR, Khokhlova VA. Compensation for aberrations of focused ultrasound beams in transcranial sonications of brain at different depths. Acoust Phys 2022;68:1–10. doi: 10.1134/S1063771022010018.
[40] Ali R, Brevett T, Zhuang L, Bendjador H, Podkowa AS, Hsieh SS, et al. Aberration correction in diagnostic ultrasound: a review of the prior field and current directions. Z Med Phys 2023;33:267–91. doi: 10.1016/j.zemedi.2023.01.003.
[41] Soulioti DE, Espindola D, Dayton PA, Pinton GF. Super-resolution imaging through the human skull. IEEE Trans Ultrason Ferroelectr Freq Control 2020;67:25–36. doi: 10.1109/TUFFC.2019.2937733.
[42] Bureau F, Robin J, Le Ber A, Lambert W, Fink M, Aubry A. Three-dimensional ultrasound matrix imaging. Nat Commun 2023;14:6793.. doi: 10.1038/s41467-023-42338.
[43] Song M, Thomas GPL, Khokhlova VA, Sapozhnikov OA, Bailey MR, Maxwell AD, et al. Quantitative assessment of boiling histotripsy progression based on color Doppler measurements. IEEE Trans Ultrason Ferroelectr Freq Control 2022;69:3255–69. doi: 10.1109/TUFFC.2022.3212266.